APL Materials

RESEARCH ARTICLE | APRIL 03 2023

Silicon-doped β-Ga_2O_3 films grown at 1 μm/h by suboxide molecular-beam epitaxy

Kathy Azizie ; Felix V. E. Hensling ; Cameron A. Gorsak ; Yunjo Kim; Naomi A. Pieczulewski; Daniel M. Dryden ; M. K. Indika Senevirathna ; Selena Coye; Shun-Li Shang; Jacob Steele ; Patrick Vogt ; Nicholas A. Parker; Yorick A. Birkhölzer ; Jonathan P. McCandless; Debdeep Jena ; Huili G. Xing ; Zi-Kui Liu; Michael D. Williams ; Andrew J. Green; Kelson Chabak; David A. Muller ; Adam T. Neal ; Shin Mou; Michael O. Thompson ; Hari P. Nair; Darrell G. Schlom

APL Mater 11, 041102 (2023)
https://doi.org/10.1063/5.0139622

Silicon-doped β-Ga_2O_3 films grown at 1 μm/h by suboxide molecular-beam epitaxy

Cite as: APL Mater. 11, 041102 (2023); doi: 10.1063/5.0139622
Submitted: 21 December 2022 • Accepted: 24 February 2023 •
Published Online: 3 April 2023

Kathy Azizie,[1] Felix V. E. Hensling,[1] Cameron A. Gorsak,[1] Yunjo Kim,[2] Naomi A. Pieczulewski,[1] Daniel M. Dryden,[3] M. K. Indika Senevirathna,[4] Selena Coye,[4] Shun-Li Shang,[5] Jacob Steele,[1] Patrick Vogt,[1] Nicholas A. Parker,[1] Yorick A. Birkhölzer,[1] Jonathan P. McCandless,[6] Debdeep Jena,[1,6,7] Huili G. Xing,[1,6,7] Zi-Kui Liu,[5] Michael D. Williams,[4] Andrew J. Green,[3] Kelson Chabak,[3] David A. Muller,[7,8] Adam T. Neal,[2] Shin Mou,[2] Michael O. Thompson,[1] Hari P. Nair,[1] and Darrell G. Schlom[1,7,9,a)]

AFFILIATIONS

[1] Department of Materials Science and Engineering, Cornell University, Ithaca, New York 14853, USA
[2] Air Force Research Laboratory, Materials and Manufacturing Directorate, Wright Patterson Air Force Base, Ohio 45433, USA
[3] Air Force Research Laboratory, Sensors Directorate, Wright Patterson Air Force Base, Ohio 45433, USA
[4] Department of Physics, Clark Atlanta University, Atlanta, Georgia 30314, USA
[5] Department of Material Science and Engineering, Pennsylvania State University, University Park, Pennsylvania 16802, USA
[6] School of Electrical and Computer Engineering, Cornell University, Ithaca, New York 14853, USA
[7] Kavli Institute at Cornell for Nanoscale Science, Ithaca, New York 14853, USA
[8] School of Applied and Engineering Physics, Cornell University, Ithaca, New York 14853, USA
[9] Leibniz-Institut für Kristallzüchtung, Max-Born-Str. 2, 12489 Berlin, Germany

[a)] **Author to whom correspondence should be addressed:** schlom@cornell.edu

ABSTRACT

We report the use of suboxide molecular-beam epitaxy (*S*-MBE) to grow β-Ga_2O_3 at a growth rate of ~1 μm/h with control of the silicon doping concentration from 5×10^{16} to 10^{19} cm^{-3}. In *S*-MBE, pre-oxidized gallium in the form of a molecular beam that is 99.98% Ga_2O, i.e., gallium suboxide, is supplied. Directly supplying Ga_2O to the growth surface bypasses the rate-limiting first step of the two-step reaction mechanism involved in the growth of β-Ga_2O_3 by conventional MBE. As a result, a growth rate of ~1 μm/h is readily achieved at a relatively low growth temperature ($T_{sub} \approx 525\,^{\circ}C$), resulting in films with high structural perfection and smooth surfaces (rms roughness of <2 nm on ~1 μm thick films). Silicon-containing oxide sources (SiO and SiO_2) producing an SiO suboxide molecular beam are used to dope the β-Ga_2O_3 layers. Temperature-dependent Hall effect measurements on a 1 μm thick film with a mobile carrier concentration of 2.7×10^{17} cm^{-3} reveal a room-temperature mobility of 124 cm^2 V^{-1} s^{-1} that increases to 627 cm^2 V^{-1} s^{-1} at 76 K; the silicon dopants are found to exhibit an activation energy of 27 meV. We also demonstrate working metal–semiconductor field-effect transistors made from these silicon-doped β-Ga_2O_3 films grown by *S*-MBE at growth rates of ~1 μm/h.

INTRODUCTION

With its very high bandgap, dopability, good mobility for electrons, and the availability of a large-diameter native substrate, β-Ga_2O_3 has emerged as a promising material for high-power electronics.[1,2] Although molecular-beam epitaxy (MBE) is the leading technique for the growth of most compound semiconductors, for the growth of β-Ga_2O_3, it has serious limitations, and metalorganic chemical vapor deposition (MOCVD) is currently the method

of choice.[3,4] A direct comparison of the best electrical properties reported for the growth of β-Ga_2O_3 films by MBE[5,6] and MOCVD[3] at growth rates near current limits for each is shown in Table I, revealing the shortcomings of MBE.

The conventional MBE growth of β-Ga_2O_3 starts with metallic gallium, which undergoes a two-step reaction to form solid Ga_2O_3,[7–9]

$$2\,\mathrm{Ga} + \mathrm{oxidant} \rightarrow \mathrm{Ga_2O} + \mathrm{additional\,oxidant} \rightarrow \mathrm{Ga_2O_3}, \quad (1)$$

where the oxidant is either oxygen plasma or ozone. The suboxide produced in the first step, Ga_2O, is volatile at typical growth temperatures, and if there is insufficient oxidant present to oxidize it, it will desorb from the substrate surface diminishing the throughput of the second step. The first step is rate-limiting and even operating at the oxidant pressure limit that hot filaments in an MBE can withstand, i.e., ~10^{-5} Torr, the growth rate of β-Ga_2O_3 is relatively slow, in the ~0.1 μm/h range.[2,5,6] It is possible to enhance this meager growth rate by catalytic means[10] using a process referred to as metal-oxide catalyzed epitaxy (MOCATAXY)[11] or metal-exchange catalyzed molecular beam epitaxy (MEXCAT-MBE).[12] The metallic catalyst can be added indium, which can be incorporated into β-$(Al_xGa_{1-x})_2O_3$ films at the ~1% level[11] or through the addition of a dopant, e.g., tin.[13] Another way to increase the growth rate is to bypass the first step of the two-step reaction mechanism and directly supply an incident molecular beam of Ga_2O, i.e., suboxide MBE (*S*-MBE),[14] rather than by supplying a molecular beam of gallium.

Using *S*-MBE increases the growth rate by overcoming the kinetic limits imposed by the first reaction shown in Eq. (1), leading to an order of magnitude higher growth rate in the ~1 μm/h range.[14] There are a couple of options to produce a molecular beam of Ga_2O suboxide. One is to use solid Ga_2O_3 itself,[15,16] and the other is to use a mixture of solid Ga_2O_3 and liquid gallium.[17] Vapor pressure calculations show that the dominant species in the molecular beam for both methods is the suboxide Ga_2O.[18,19] An advantage, however, of using the Ga_2O_3 + gallium mixture is the far lower temperature needed to produce the Ga_2O molecular beam.[18,19] This allows more types of crucibles to be used to contain the mixture (e.g., Al_2O_3 and BeO crucibles), increases the Ga_2O flux that can be achieved (and with it the growth rate of the β-Ga_2O_3 film), and decreases contaminants coming from the hot crucible and effusion cell. For example, when solid Ga_2O_3 has been used as a source, even at source temperatures in the 1700 °C range, the maximum growth rate that has been achieved is 0.14 μm/h and the films have been contaminated with ~5 × 10^{18} iridium atoms cm^{-3} coming from the iridium crucible used to contain the very hot Ga_2O_3 source.[20–22] In contrast, films of β-Ga_2O_3 produced using *S*-MBE using a Ga_2O_3 + gallium mixture result in growth rates exceeding 1 μm/h, excellent crystallinity, and smooth surfaces all at a relatively low growth temperature, T_{sub}.[14] The disadvantage of *S*-MBE is that generating a Ga_2O molecular beam at low temperatures utilizes a source containing a mixture of Ga_2O_3 *powder* plus gallium metal.[14,17] Unfortunately, the highest purity of Ga_2O_3 powder that we are able to obtain commercially is only 99.999% (5N), whereas 99.99999% (7N) pure gallium is the norm for conventional MBE. This lower purity raises questions about whether *S*-MBE can grow device-quality films. The direct way to answer this question is to make devices on β-Ga_2O_3 layers grown by *S*-MBE and see how they perform.

Studying the mobility of β-Ga_2O_3 films and fabricating β-Ga_2O_3-based devices necessitate controlled doping. Silicon is the preferred dopant for β-Ga_2O_3 films as it not only yields films with highest mobility[2,3,23–25] but has been demonstrated to provide abrupt and controlled doping over the 10^{16}–10^{20} cm^{-3} range in β-Ga_2O_3 films grown by MOCVD.[2,3,24–27] Silicon segregates less to the surface during the MBE growth than does tin,[6] making it a superior dopant, and it has the advantage over germanium of a far lower diffusion coefficient in β-Ga_2O_3 at temperatures required for device processing.[28] The traditional MBE approach to dope with silicon is to create a silicon molecular beam by heating silicon to high temperatures in an MBE source. Unfortunately, in the high oxidant pressure (~10^{-5} Torr) used for the growth of β-Ga_2O_3 by MBE, the surface of the silicon doping source may also oxidize.[29] Whether the silicon surface gets covered over by a layer of SiO_2 or is able to desorb gaseous SiO at the same rate that the silicon source is oxidized and, thus, remain uncoated depends on the temperature of the silicon and the oxidant pressure. For the case that the oxidant pressure is fixed at 1 × 10^{-5} Torr, at high temperatures ($T_{Si} \gtrsim 830$°C), the silicon surface is able to desorb all of the oxide that forms and remains clean, whereas at low temperature, ($T_{Si} \lesssim 830$°C), the silicon surface gets coated by solid SiO_2.[30–32] These changes with the oxidation of the silicon source result in huge changes in the flux of silicon or SiO emanating from the silicon source, thwarting controlled and reproducible doping at device-relevant concentrations.[4,5,29]

This paper tackles the challenges of growing silicon-doped β-Ga_2O_3 thin films by taking advantage of the suboxide forms of both silicon and gallium. In this work, we demonstrate both controllable and reproducible silicon doping of β-Ga_2O_3 at device-relevant

TABLE I. Comparison of the highest reported electrical mobilities of β-Ga_2O_3 films grown at a relatively high rate by MBE vs MOCVD.

	Mobility at room temperature ($cm^2\,V^{-1}\,s^{-1}$)	Peak mobility ($cm^2\,V^{-1}\,s^{-1}$)	Temperature of peak mobility(K)	Growth rate (μm/h)	Range of controlled doping (cm^{-3})	References
MBE[a]	129	390	97	0.09	10^{17}–10^{20}	5
MBE[b]	136	168	165	0.3	4×10^{16}–2×10^{19}	6
MOCVD	190	3425	53	2.9	2×10^{16}–4×10^{19}	3

[a]Conventional plasma-assisted MBE.
[b]Metal-oxide catalyzed epitaxy (MOCATAXY).

concentrations, i.e., the 5×10^{16}–10^{19} cm^{-3} range, with a growth rate of ~1 μm/h by *S*-MBE. Having overcome the doping challenge, we then evaluate the mobility of the silicon-doped β-Ga_2O_3 layers and demonstrate working devices made by *S*-MBE at a growth rate of ~1 μm/h.

EXPERIMENTAL

All films were grown using a Veeco GEN10 MBE system equipped with retractable and differentially pumped effusion cells that can be exchanged without venting the entire MBE system. This facilitates refilling the Ga_2O_3 + gallium source. The film growth took place on (0001)-oriented sapphire substrates (Kyocera) or (010)-oriented iron-doped β-Ga_2O_3 single-crystal substrates (Novel Crystal Technology) with $10 \times 10 \times 0.5$ mm^3 dimensions held in substrate holders made of Haynes® 214® alloy. The backside of each substrate was coated with a ~200 nm thick platinum layer (on top of a ~20 nm thick titanium adhesion layer) to enable it to be radiatively heated by an SiC heating element to T_{sub} = 525 or 550 °C as measured by an optical pyrometer operating at a wavelength of 980 nm.

A detailed description of the thermodynamics and kinetics of the growth of Ga_2O_3 by suboxide MBE is given in prior publications.[14,33] Thermodynamic calculations in the present work were performed using the Scientific Group Thermodata Europe (SGTE) Substance Database (SSUB5)[34] within the Thermo-Calc software.[35]

To obtain a molecular beam of gallium suboxide, we shake the combination of Ga_2O_3 powder (Alfa Aesar, 99.999% purity) and molten metallic gallium (Alfa Aesar, 99.99999% purity) to produce a mixture with a molar fraction of oxygen of $x(O) = 0.4$. The Ga_2O_3 + gallium charge is contained within a beryllium oxide (BeO) crucible (Materion, 99.7% purity) in the MBE effusion cell. Our thermodynamic calculations estimate that such a mixture heated to the 750–1000 °C range of temperatures used in this study will produce a molecular beam that is 99.98% Ga_2O.[14] Films were grown at a background pressure of distilled ozone (~80% ozone with the balance being O_2) of $P_{O3} = (1–5) \times 10^{-6}$ Torr. The growth rate of films grown on *c*-axis sapphire substrates was determined by measuring the thicknesses of the β-Ga_2O_3 films by x-ray reflectivity (XRR). For films grown on (010)-oriented iron-doped β-Ga_2O_3 single-crystal substrates, the growth rate was estimated by growing calibration films on *c*-axis sapphire substrates and assuming that the growth rate was the same on the (010)-oriented β-Ga_2O_3 substrates. The thickness of one sample (sample a) was measured by scanning transmission electron microscopy (STEM) and found to be ~40% thicker than this simple estimation. For two of the homoepitaxial β-Ga_2O_3 films (samples k and l), the growth rate was established by depth measurements made using a stylus profilometer on secondary-ion mass spectrometry (SIMS) craters.

To dope silicon into β-Ga_2O_3 films, we tried two silicon-containing oxide sources: SiO (Alfa Aesar, 99.99% purity) and SiO_2 (Kurt J. Lesker, 99.99% purity) contained within Al_2O_3 crucibles (McDanel, 99.8% purity). From vapor pressure calculations, both sources are expected to produce a molecular beam of suboxide SiO.[19] This approach is an attempt to circumvent the challenges associated with going back and forth between the active and passive oxidation regimes of elemental silicon as the silicon source temperature is changed, as unfortunately occurs in the growth of β-Ga_2O_3 by conventional MBE using a silicon source.[5,29] Both SiO and SiO_2 have previously been used as doping sources for silicon in oxide MBE: SiO to dope β-Ga_2O_3 films[36,37] and SiO_2 to dope α-Al_2O_3 films.[38]

The SiO_x flux emanating from the SiO and SiO_2 doping sources was measured in two ways. At high SiO and SiO_2 source temperatures, where the SiO_x flux was sufficient to build up a multi-nanometer thick film in a reasonable time, its thickness was determined by XRR. XRR measurements were made on amorphous SiO_x films deposited on unheated (0001) Al_2O_3 or (100) MgO substrates using the calibration scheme described by Ref. 37. The silicon fluxes calculated from these XRR measurements were independent of the oxidant employed for background pressures of distilled ozone ranging from none (vacuum) up to at least 2.5×10^{-6} Torr. At lower SiO and SiO_2 source temperatures, the SiO_x flux was inferred from Hall effect measurements of silicon-doped β-Ga_2O_3 films. The Hall effect measurements were made using a van der Pauw geometry[39] with four ohmic contacts on 1 μm thick silicon-doped β-Ga_2O_3 films grown by *S*-MBE at a growth rate of ~1 μm/h on iron-doped β-Ga_2O_3 (010) substrates that were $10 \times 10 \times 0.5$ mm^3 in size. For highly silicon-doped samples (greater than 1×10^{19} cm^{-3}), contacts to the films were made by soldering indium at the corners. In order to make ohmic contact to more lightly silicon-doped films, ~90 nm of n^+ epitaxial β-Ga_2O_3 was regrown on the four corners of the films using a shadow mask in an Agnitron Agilis 100 MOCVD system. The donor density (N_d) in these n^+ layers was greater than 1×10^{19} cm^{-3} to ensure that the contacts are ohmic. The MOCVD reactor pressure was 50 Torr, and the substrate temperature was 630 °C. Triethylgallium (TEGa), oxygen (99.999%), and silane (25 ppm SiH_4 in argon) were used as precursors, with argon (99.999%) as the carrier gas. Then, indium was soldered on top of the regrown n^+ β-Ga_2O_3 contacts. A Nanometrics HL5500 Hall system was used on these samples to determine the sheet carrier concentration of mobile charges at room temperature. The silicon flux was estimated under the assumption that all silicon is activated at room temperature in the β-Ga_2O_3 film. The temperature-dependent transport properties of select samples (samples a, b, and d) were measured as a function of temperature using a vacuum cryostat with a closed-cycle helium compressor and an electromagnet with an applied magnetic field of 0.5 T for Hall-effect measurements.

X-ray diffraction (XRD) and x-ray reflectivity (XRR) measurements were performed in a coplanar symmetric geometry using a PANalytical Empyrean system equipped with a copper anode and a hybrid incident-beam monochromator to provide Cu $K_{\alpha 1}$ radiation. Rocking curves were collected in a triple-axis configuration using a 220 Ge analyzer crystal. An Asylum Research Cypher ES atomic force microscope (AFM) was used to measure the surface roughness.

SIMS measurements were made either using a Hiden Analytical SIMS Plus Workstation or by EAG Laboratories. The Hiden Analytical SIMS Plus Workstation used an O_2^+ ion source as the primary beam to profile the sample. The system features a MAXIM quadrupole mass analyzer to detect and analyze the emitted secondary ions at 30° to the probe axis. The O_2^+ primary ion beam was oriented at 45° relative to the sample surface. The primary beam voltage and current for the analysis were 2 kV and 140 nA, respectively. The crater area, scan density, electronic gate, and oxygen flooding pressure were 400×400 μm^2, 100×100 $pixels^2$, 5% of the

raster area, and 4.0×10^{-6} Torr, respectively. The SIMS system base pressure was ~5.0×10^{-10} Torr.

The microstructure of one epitaxial β-Ga_2O_3 film (sample a) was examined using STEM. The sample was prepared in the cross-sectional geometry perpendicular to the $[\bar{2}01]$ direction and thinned to electron transparency using a Thermo Fisher Helios G4 UX focused ion beam with a final milling step of 5 keV to minimize the damage of the top layer. Carbon and platinum protective layers were deposited on the sample prior to milling to minimize the ion-beam damage. STEM measurements were taken with an aberration-corrected Thermo Fisher Spectra 300 CFEG operated at 300 keV with a high-angle annular dark-field (HAADF) detector.

Metal–semiconductor field-effect transistors (MESFETs) were fabricated using annealed Ti/Al/Ni/Au ohmic contacts, a Ni/Au gate, and mesa isolation via reactive-ion etching,[40] with a channel length of 3 μm and a gate length of 1 μm.

RESULTS AND DISCUSSION

Utilizing a Ga_2O_3 + gallium two-phase mixture to produce a molecular beam of the suboxide Ga_2O, we first map out the growth rate of β-Ga_2O_3 on (0001) Al_2O_3 substrates as a function of suboxide flux under conditions yielding epitaxial films. In Fig. 1, we demonstrate that the growth rate of β-Ga_2O_3 is a function of substrate temperature, distilled ozone pressure, and Ga_2O flux. For a constant substrate temperature and background pressure of distilled ozone, the growth rate, at first, increases linearly with the Ga_2O flux and then plateaus. This behavior is seen in Fig. 1(a). For the growth conditions studied, the β-Ga_2O_3 films grown on (0001) Al_2O_3 were fully epitaxial by reflection high-energy electron diffraction and XRD with $(\bar{2}01)$ orientation in agreement with prior reports of the growth of β-Ga_2O_3 on (0001) Al_2O_3 by pulsed-laser deposition,[41] MOCVD,[42] conventional MBE,[7,8,37,43,44] and *S*-MBE.[14–16] The linear region corresponds to oxidant-rich conditions, where all of the Ga_2O supplied in the incident flux is oxidized to Ga_2O_3 during its residence time on the substrate surface. When the Ga_2O flux increases further—into the Ga_2O-rich regime—the excess Ga_2O, beyond what can be oxidized by the background pressure of the distilled ozone, is desorbed from the surface due to the volatility of Ga_2O at the substrate temperatures employed. This results in a plateau in the growth rate with increasing gallium suboxide Ga_2O flux. The growth rate in the plateau regime depends solely on the background pressure of the distilled ozone (and substrate temperature); it is an adsorption-controlled growth regime, where the insufficient ozone flux limits the adsorption of the excess Ga_2O flux. As the background ozone pressure is increased, more Ga_2O can be oxidized during its residence time and the growth rate is found to increase. This occurs by an extension of the oxidant-rich (linear) regime to a new plateau of the growth rate at a higher Ga_2O flux, beyond which there is insufficient ozone present to oxidize all of the Ga_2O to Ga_2O_3 during its residence time on the substrate surface. At a substrate temperature of 525 °C and a background distilled ozone pressure of $P_{O3} = 5 \times 10^{-6}$ Torr, we achieve growth rates as high as 2.5 μm/h on (0001) Al_2O_3. Similarly, when keeping the ozone pressure constant and varying the substrate temperature, the growth rate is seen [Fig. 1(b)] to decrease with increasing substrate temperature due to the decreased residence time of the Ga_2O on the substrate surface as the substrate temperature is increased. The oxidant-rich and adsorption-controlled growth regimes are still observed, just shifted due to the change in the residence time. These results agree with a kinetic model developed for *S*-MBE.[14,33]

Having established the conditions for the epitaxial growth of β-Ga_2O_3 films at a rate of ~1 μm/h, we next consider doping them with silicon. For this purpose, we tried both of the oxides of silicon, first SiO and then SiO_2, as source materials to dope β-Ga_2O_3. To calibrate the flux of the SiO molecular beam, XRR was used to determine the growth rate of amorphous SiO_x films. As XRR provides a measure of both the film thickness and the film density,[45] the

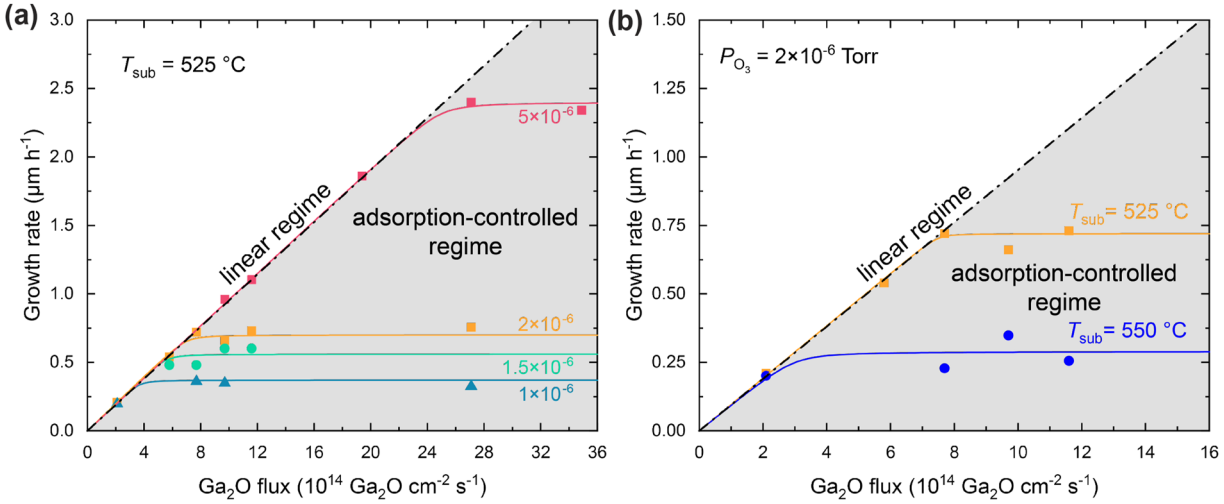

FIG. 1. Growth rate of β-Ga_2O_3 on (0001) Al_2O_3 substrates as a function of Ga_2O flux. (a) Growth rate at a constant substrate temperature (T_{sub} = 525 °C) at four different background pressures (in Torr) of distilled ozone showing the oxidant-rich (linear) regime and the Ga_2O-rich (adsorption-controlled) regime. (b) The effect of substrate temperature on the growth rate. The smooth curves indicate a fit to the experimental growth rates by the kinetic model described in Ref. 33.

XRR spectra of smooth SiO_x films enable the silicon flux to be calculated as a function of temperature of the SiO source, T_{SiO}. From the XRR spectra, the density of the amorphous SiO_x films deposited by the SiO source was about 1.8 g/cm^3, comparable to that reported in prior studies of vacuum-deposited SiO_x films deposited under similar conditions.[37,46] To evaluate the stability of the SiO source and the associated reproducibility of growing silicon-doped β-Ga_2O_3 films over a range of desired conditions, we grew amorphous SiO_x calibration films at oxidant pressures ranging from vacuum to $P_{O3} = 5 \times 10^{-6}$ Torr. While the SiO source behaved well at the high values of T_{SiO} used for the growth of the XRR samples, at the lower values of T_{SiO} relevant to doping β-Ga_2O_3 films with silicon concentrations in the 10^{17}–10^{19} cm^{-3} range, SIMS measurements revealed a major challenge with using SiO as a source. At a lower T_{SiO}, the flux is not reproducible. Not only did doping at the same value of T_{SiO} vary considerably from growth to growth (as seen in Hall measurements), but often, the doping concentrations measured in SIMS stacks would not follow an Arrhenius relationship as T_{SiO} was varied. Presumably, this is due to the surface of the SiO forming an SiO_2 crust in the presence of ozone, causing the flux to plummet. This is consistent with the results reported by Ardenghi *et al.*[37] for SiO used in conjunction with an oxygen plasma in the growth of silicon-doped β-Ga_2O_3 by plasma-assisted MBE (PAMBE). For this reason, we found SiO to be unsuitable as a controlled and reproducible doping source and moved on to evaluating SiO_2 for this purpose.

In calibrating the SiO_2 source, XRR measurements of amorphous SiO_x on (0001) Al_2O_3 substrates revealed that a well-behaved and reproducible silicon flux emanates from it, despite changing the oxidant pressure from vacuum to $P_{O3} = 2.5 \times 10^{-6}$ Torr. From the XRR spectra, the density of the amorphous SiO_x films deposited by the SiO_2 source was about 2.1 g/cm^3 as tabulated for each sample in the supplementary material (Table S1). Having established that the SiO_2 source performed well when its temperature, T_{SiO2}, was high, we moved on to evaluating its stability at lower T_{SiO2} relevant to doping β-Ga_2O_3 films. For these lower fluxes of the silicon-containing dopant species (mainly SiO from vapor pressure calculations[19]), Hall measurements were performed on silicon-doped homoepitaxial β-Ga_2O_3 films in both the oxidant-rich and adsorption-controlled regimes. The silicon flux is determined from the Hall measurements assuming full activation at room temperature, an assumption that may underestimate the silicon flux. On the other hand, mobile carriers due to the unintentional silicon contamination that often occurs at the interface between the β-Ga_2O_3 film and the underlying substrate[14,25,47–49] could lead to the Hall measurements overestimating the silicon flux. Tables II and S1 (supplementary material) list the growth conditions of the samples grown using an SiO_2 source. Table II lists the samples investigated by Hall measurements (samples a–l), while Table S1 lists the samples measured by XRR (samples o–v).

Figure 2 shows an Arrhenius plot of the silicon flux calculated from both the XRR and Hall data as a function of T_{SiO2}. A clear Arrhenius behavior with an activation energy of about 5 eV is seen between the silicon flux and $1/T_{SiO2}$. To assess our ability to control silicon doping over the 10^{16}–10^{19} cm^{-3} range using the SiO_2 suboxide doping source, we attempted to grow two 7 μm thick films for SIMS analysis, one in the oxidant-rich regime and the other in the adsorption-controlled regime. Each film starts off with a 1 μm thick undoped β-Ga_2O_3 buffer layer followed by alternating 0.5 μm thick layers of silicon-doped and undoped β-Ga_2O_3 as shown by the schematics in Figs. 3(a) and 3(c) for the SIMS stacks grown in the oxidant-rich and adsorption-controlled regimes, respectively. To keep the growth conditions similar and yet explore the two growth regimes to see whether they affect the dopant incorporation or the doping profile in some way, both SIMS stacks were grown at the same $T_{sub} = 525\,^{\circ}C$ and the same $P_{O3} = 2.5 \times 10^{-6}$ Torr. Accessing the oxidant-rich regime vs the adsorption-controlled regimes was achieved by using different Ga_2O fluxes for these two SIMS stacks: 6×10^{14} molecules cm^{-2} s^{-1} for the oxidant-rich regime and 1×10^{15}

TABLE II. Growth parameters and electrical characteristics of the β-Ga_2O_3 films measured by the Hall effect and SIMS.[a]

Name	Mobility (cm^2 V^{-1} s^{-1})	Carrier density (cm^{-3})	SiO_2 source temperature (°C)	Thickness (nm)	Ga_2O flux (molecules cm^{-2} s^{-1})
Sample a	124	2.7×10^{17}	1286	1000	1×10^{15}
Sample b	119	2.9×10^{17}	1134	1000	6×10^{14}
Sample c	111	3.5×10^{17}	1115	1000	6×10^{14}
Sample d	129	3.5×10^{17}	1119	1000	1×10^{15}
Sample e	104	9.8×10^{17}	1187	1000	6×10^{14}
Sample f	86	1.3×10^{18}	1225	1000	1×10^{15}
Sample g	98	1.5×10^{18}	1171	1000	6×10^{14}
Sample h	91	2.4×10^{18}	1176	1000	1×10^{15}
Sample i	75	5.5×10^{18}	1262	1000	1×10^{15}
Sample j	79	1.1×10^{19}	1286	1000	1×10^{15}
Sample k	62	3.0×10^{19}	1319	1000	1×10^{15}
Sample l	68	4.4×10^{19}	1350	1000	1×10^{15}
Sample m	⋯	⋯	Figure 3(a)	6500	6×10^{14}
Sample n	⋯	⋯	Figure 3(c)	9000	1×10^{15}

[a]All samples were grown at $T_{sub} = 525\,^{\circ}C$ in $P_{O3} = 2.5 \times 10^{-6}$ Torr on iron-doped (010) β-Ga_2O_3 substrates and doped with an SiO_2 source.

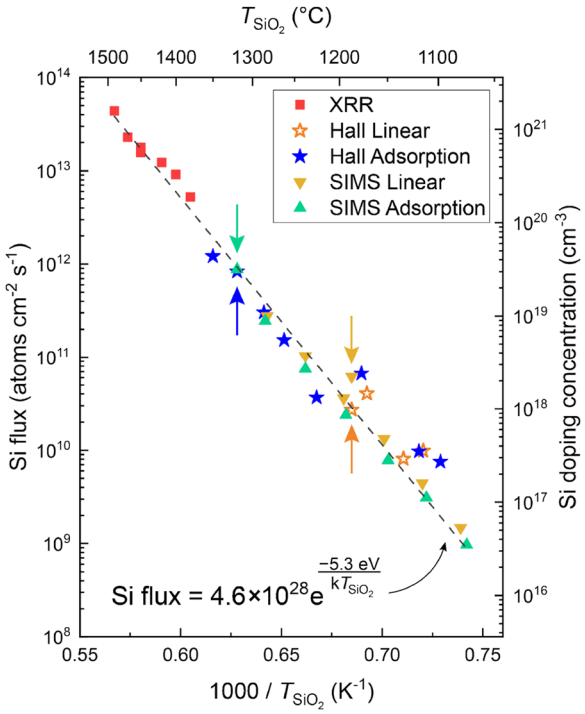

FIG. 2. Silicon flux incorporated into β-Ga_2O_3 films as measured by XRR (red squares), SIMS (triangles), and the Hall effect (stars) as a function of the temperature of the SiO_2 doping source (T_{SiO2}). The linear fit shown is calculated based on the XRR and SIMS data points, where T_{SiO2} is in kelvin. Two of the samples on which the Hall effect was measured were also measured by SIMS. For those two samples, the calculated silicon flux values are indicated by the vertical arrows, showing that the fraction of silicon that is electrically active is lower when the β-Ga_2O_3 is less highly doped. The vertical axis on the right side of the figure gives the silicon doping concentration that the silicon flux would produce in a film of β-Ga_2O_3 grown at 1 μm/h.

molecules cm^{-2} s^{-1} for the adsorption-controlled regime [Fig. 1(a)]. The growth rates in these two regimes for the growth conditions used differ (0.86 vs 1.3 μm/h), requiring different T_{SiO2} values. During the growth of each undoped layer, the temperature of the SiO_2 source is increased to provide the silicon flux targeted for the next silicon-doped layer.

Figures 3(b) and 3(d) are the resulting SIMS measurements depicting the concentration of elements of interest—silicon, iron, aluminum, and beryllium—with respect to the sputtered depth. The SIMS data show clear and well-defined steps, demonstrating controllable silicon-doping from 5 × 10^{16} atoms cm^{-3} to 1 × 10^{19} atoms cm^{-3}. The steepness of the step edges of the silicon profile differs between the oxidant-rich and adsorption-controlled regimes, with the oxidant-rich regime consistently showing sharper steps. The underlying reason could be the increased rms roughness of the ~9 μm thick SIMS stack grown in the adsorption-controlled regime (53 nm) in comparison with the ~6.5 μm thick SIMS stack grown in the oxidant-rich regime (11 nm). We also note that when the silicon shutter is open, the silicon profile is also observed to be flatter for the oxidant-rich regime [Fig. 3(b)], whereas it has a slight upward slope (indicative of silicon riding the surface) for the adsorption-controlled regime [Fig. 3(d)].

Despite calibrating the silicon incorporation by XRR and Hall measurements, the silicon concentration measured by SIMS in Figs. 3(b) and 3(d) does not precisely match the incorporation targeted in our SIMS stack design in Figs. 3(a) and 3(c). At high silicon-doping (T_{SiO2} > 1187 °C), the match is good, but at lower T_{SiO2}, the concentration observed by SIMS is lower than the predicted silicon incorporation by up to a factor of 5. One explanation of this discrepancy is that the Hall data overestimate the silicon concentration at low doping because of the unintentional silicon contamination at the substrate interface[14,25,47–49] giving rise to a concentration of mobile carriers beyond that provided by the silicon flux during growth. To assess this hypothesis, additional SIMS measurements were conducted on two Hall samples (samples k and e), one in each growth regime. If this hypothesis were true, then the concentration of silicon measured by SIMS should be less than the mobile carrier concentration measured on the same samples by the Hall effect. The results are shown in Fig. 2, where the vertical arrows point to the silicon fluxes measured by SIMS and Hall effect on the same sample. The data do not support the hypothesis. Rather, the data show that the silicon concentration measured by SIMS is as large as or larger than the concentration measured by the Hall effect. The data show that at high doping, almost all of the silicon is electrically active, ~90% at 3 × 10^{19} cm^{-3} doping. At lower doping, however, the fraction of silicon dopants that produce mobile carriers is far lower, with ~40% activation of silicon at 2 × 10^{18} cm^{-3} doping. This could be from a background of compensating acceptor states in our films, but the concentration involving ~10^{18} cm^{-3} of acceptors or traps is so high that it is inconsistent with the relatively high mobilities seen in other films as we describe below.

The concentration of silicon incorporated into the β-Ga_2O_3 films as a function of T_{SiO2} in the SIMS stacks shown in Figs. 3(b) and 3(d) was used to calculate the silicon flux at doping-relevant temperatures and is also plotted in Fig. 2. From these SIMS values and the XRR values, a more accurate fit to the Arrhenius behavior between the silicon flux and 1/T_{SiO2} can be obtained. Unlike the Hall measurement, which only probes mobile carriers, the SIMS and XRR data measure all of the silicon incorporated. The resulting best fit has an activation energy of 5.3 eV/molecule. Although some scatter exists, particularly between Hall and SIMS values, the results in Fig. 2 show a linear trend that extends over 5 orders of magnitude, establishing that SiO_2 is a well-behaved doping source for the growth of β-Ga_2O_3 by suboxide MBE. We attribute the more stable behavior of the SiO_2 doping source over an SiO or silicon doping source to the fact that SiO_2 is fully oxidized and free of the active/passive oxidation issues[30–32] that plague SiO[37] and silicon[5,29] sources when used at the high oxidant pressures involved in the growth of β-Ga_2O_3 by MBE.

In addition to measuring the concentration of silicon, the concentrations of iron, aluminum, and beryllium were also measured by SIMS. This is because these elements are the major impurities in our Ga_2O_3 powder or they are the major constituents of the BeO and Al_2O_3 crucibles used to contain the Ga_2O_3 + gallium mixture and SiO_2 sources, respectively. A composition analysis on the 99.999% Ga_2O_3 powder reveals aluminum, boron, sodium, and iron to be the only elements present at above the ppm level. A broad screening of these elements and more by SIMS analysis (not shown) indicated

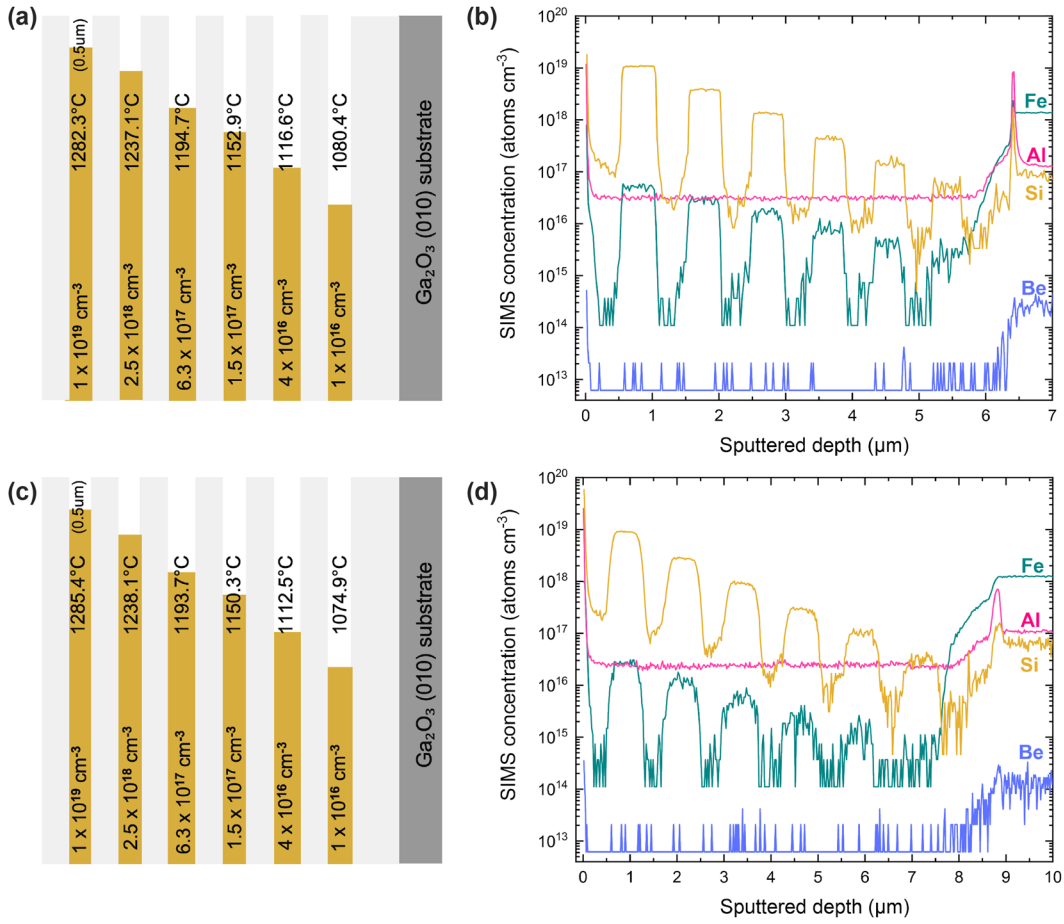

FIG. 3. SIMS profiles showing the concentrations of silicon, iron, aluminum, and beryllium as a function of depth of silicon-doped β-Ga_2O_3 films grown at T_{sub} = 525 °C and a background oxidant pressure of 2.5 × 10^{-6} Torr of distilled ozone. (a) Schematic of the targeted doping profile, including T_{SiO2} for each layer, and (b) the measured SIMS profile of the silicon-doped β-Ga_2O_3 films grown in the oxidant-rich (linear) regime at a growth rate of 0.86 μm/h at a Ga_2O flux of 6 × 10^{14} molecules cm^{-2} s^{-1}. (c) Schematic of the targeted doping profile, including T_{SiO2} for each layer, and (d) the measured SIMS profile of the silicon-doped β-Ga_2O_3 films grown in the Ga_2O-rich (adsorption-controlled) regime at a growth rate of 1.3 μm/h at a Ga_2O flux of 1 × 10^{15} molecules cm^{-2} s^{-1}.

that the major contaminants in our undoped β-Ga_2O_3 films grown by *S*-MBE are aluminum, silicon, and iron; all impurities that are not isoelectronic with gallium have concentrations below 10^{16} cm^{-3}.[14] The low concentration of beryllium in the SIMS in Figs. 3(b) and 3(d) demonstrate that BeO is a suitable crucible for the Ga_2O_3 + gallium mixture. Of concern, however, are the high iron levels seen in Figs. 3(b) and 3(d). The steps in iron contamination seen by SIMS track the temperature changes and the shutter opening of the SiO_2 source. This indicates that the iron contamination is coming from either (1) the impurities in the SiO_2 source material, with its 99.99% purity; (2) the 99.8% pure Al_2O_3 crucible used to contain the SiO_2; or (3) the iron impurities from the iron-doped β-Ga_2O_3 substrate that ride the growth front[50] and are preferentially incorporated in the presence of silicon dopants.

When SiO_2 is heated to a temperature range of 1075–1490 °C, as is done in this work, the stable polymorph varies as is described in Fig. S1 of the supplementary material. Over this temperature range, the silicon-containing species with the highest vapor pressure is the suboxide SiO, followed by SiO_2. According to our thermodynamic calculations (Fig. S1), the SiO makes up 61% of the silicon-containing species in the gas phase at 1075 °C and 99.3% at 1490 °C. Experimentally, the dominant silicon-containing species observed in the gas phase when SiO_2 is evaporated is SiO.[51–53] Furthermore, the activation of energy of the measured vapor pressure of SiO, averaged from three studies (all with $f < 4 \times 10^{-3}$, where f is a parameter characterizing the effusion cell and, at this small magnitude, is consistent with measurements of the equilibrium vapor pressure), is 5.29 ± 0.21 eV.[51–53] This agrees well with the activation energy of 5.3 eV from the fit in Fig. 2.

Having established that SiO_2 is a well-behaved doping source, 1 μm thick films of silicon-doped β-Ga_2O_3 are grown in both the oxidant-rich and adsorption-controlled regimes at ~1 μm/h.

Figure 4(a) shows the mobility deduced from the Hall measurements of silicon-doped β-Ga_2O_3 films grown by *S*-MBE (red stars) together with the best results from the literature of silicon-doped β-Ga_2O_3 films grown by other leading techniques.[3,5,24,27,54,55] From the mobility comparison, it is evident that β-Ga_2O_3 grown by *S*-MBE with a β-SiO_2 doping source is on a par with other leading techniques. Figure 4(b) clarifies which *S*-MBE films shown in Fig. 4(a) were grown in the oxidant-rich regime and which were grown in the adsorption-controlled regime by *S*-MBE. Interestingly, there is no clear difference between the mobility at room temperature of silicon-doped β-Ga_2O_3 grown by *S*-MBE in the oxidant-rich or adsorption-controlled regime.

The sample with the highest mobility at room temperature is sample a, a 1 μm thick film grown by *S*-MBE with the SiO_2 doping source in the adsorption-controlled regime. At room temperature, it has a mobility of 124 $cm^2\ V^{-1}\ s^{-1}$. The temperature-dependence of this mobility measured by the Hall effect is shown in Fig. 5. The mobility peaks at 76 K at a mobility of 627 $cm^2\ V^{-1}\ s^{-1}$. This value is significantly higher than all prior reports of β-Ga_2O_3 grown by MBE, i.e., higher than PAMBE[5] and MOCATAXY.[6] Using the

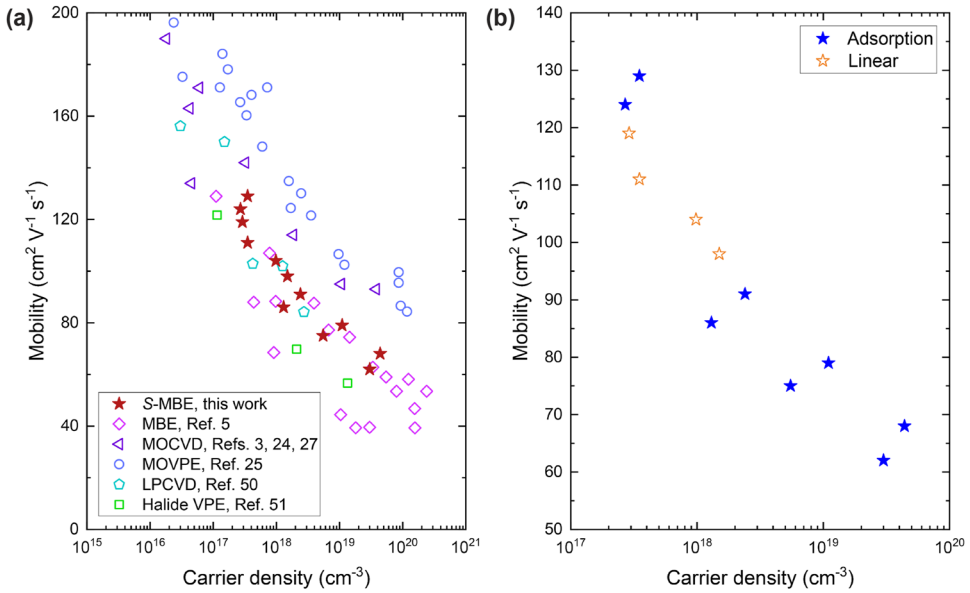

FIG. 4. (a) Comparison of the electron mobility as a function of electron density measured at room temperature by the Hall effect on the silicon-doped β-Ga_2O_3 films grown in this study at ~1 μm/h by *S*-MBE to leading reports of silicon-doped β-Ga_2O_3 films by other techniques from the literature. The *S*-MBE results are indicated by the red stars. (b) A close-up of the *S*-MBE results [the results indicated by the red stars in (a)] showing which films were grown in the oxidant-rich regime (hollow stars) and which films were grown in the adsorption-controlled regime (solid stars).

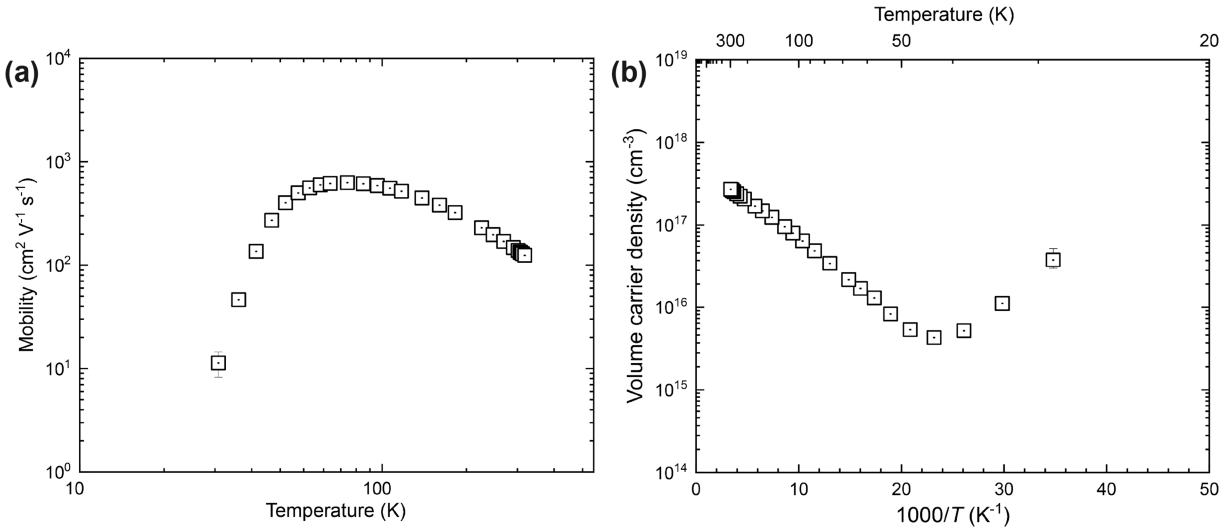

FIG. 5. Temperature-dependent Hall effect measurements made on a 1 μm thick film (sample a) grown by *S*-MBE at a growth rate of ~1 μm/h with a mobile carrier concentration of 2.7×10^{17} cm^{-3} and a room-temperature mobility of 124 $cm^2\ V^{-1}\ s^{-1}$. The mobility of the charge carriers (electrons) (a) and their density (b) are shown as a function of temperature. The mobility peaks at 76 K at a mobility of 627 $cm^2\ V^{-1}\ s^{-1}$.

temperature-dependent carrier density data for this sample as measured by the Hall effect, an activation energy of 27 meV and a compensating acceptor density (N_a) of 4×10^{15} cm^{-3} were determined by fitting the temperature-dependent Hall carrier density using the charge neutrality equation.[56,57] This activation energy for silicon from our SiO_2 doping source is comparable to that of silicon in β-Ga_2O_3 grown by conventional MBE (with an elemental silicon doping source)[5,57] and MOCVD.[3,23,25]

The results of additional structural characterization measurements on this same high-mobility sample (Sample a) are shown in Fig. 6. The film is unremarkable when analyzed by XRD; single-phase epitaxial β-Ga_2O_3 is seen. Rocking curves of the 020 β-Ga_2O_3 peak reveal full widths at half maxima (FWHMs) of 43 and 122 arcsec along two perpendicular in-plane directions. These values are on a par with the rocking curves of the bare iron-doped β-Ga_2O_3 (010) substrates. AFM reveals an rms roughness of 1.8 nm for this 1 μm thick film grown at 0.86 μm/h. High-angle annular dark-field STEM (HAADF-STEM) imaging reveals a uniform, single-crystalline β-Ga_2O_3 film with high structural quality. The thickness of the epilayer was measured to be ~1.4 μm, where the interface between the film and substrate is indicated by the black dashed line. The slight contrast at the interface likely originates from contamination at the surface of the air-exposed substrate or from point defects as has been observed in other homoepitaxial β-Ga_2O_3 films.[58] Dislocations were not observed at the film/substrate interface or in the epilayer. The variation in contrast at the surface of the film is a result of the TEM sample being prepared as a wedge that is thinner at the surface. We thus demonstrate that using *S*-MBE for both the semiconductor and the dopant tackles some of the major challenges associated with the conventional MBE growth of β-Ga_2O_3.

Having demonstrated that *S*-MBE appears to be a viable method for the growth of β-Ga_2O_3 with good structural and electrical properties at record growth rates (for MBE), we return to the question of whether it can produce device-quality materials. As an initial test, we prepared a simple MESFET on a 65 nm thick homoepitaxial β-Ga_2O_3 layer grown by *S*-MBE at a growth rate of ~1 μm/h with the structure shown in Fig. 7(a). For this test device, the SiO doping source was used to dope the epilayer. The MESFET results are shown in Figs. 7(b) and 7(c); although these are initial results, the ability of *S*-MBE to produce device-quality materials is evident. Device contacts were ohmic, and the channel showed good modulation, with a peak transconductance (G_m) of 23.4 mS/mm, threshold voltage $V_{th} \sim -6$ V, and $V_{off} = -13$ V. The relatively low on/off ratio can be attributed to the leakage through the parasitic channel formed by unintentional silicon contamination at the interface between the β-Ga_2O_3 film and the underlying substrate.[14,25,47–49] These MESFETs perform comparably to devices with similar architectures,[40,59] indicating that the

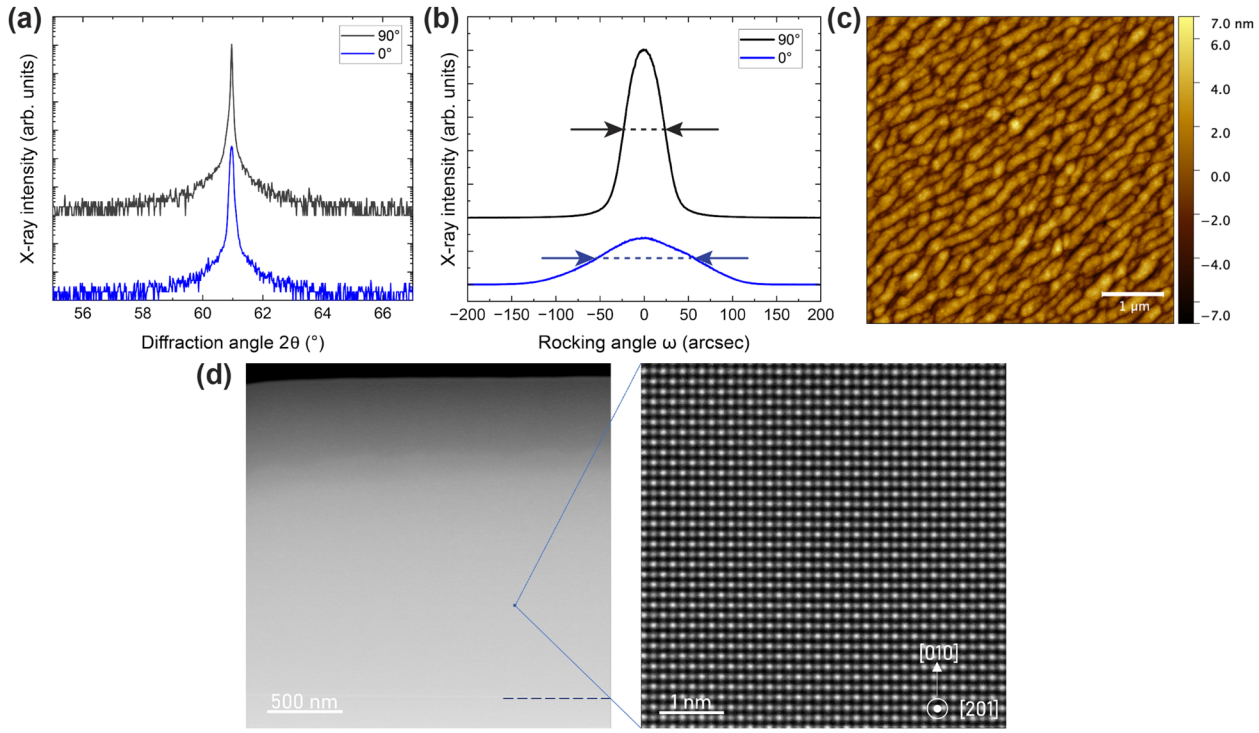

FIG. 6. Structural characterization of the same film shown in Fig. 5 by (a) θ–2θ XRD scan in the vicinity of the 020 β-Ga_2O_3 peak where the scans along $\phi = 0°$ and $\phi = 90°$ are offset for clarity. (b) Rocking curve of the 020 β-Ga_2O_3 peak showing a FWHM of 122 arcsec (blue) and 43 arcsec (gray) along $\phi = 0°$ and $\phi = 90°$, respectively; the scans are offset for clarity. (c) AFM scan of the same film revealing an rms roughness of 1.9 nm. (d) HAADF-STEM images of the same film along the [201] zone axis, where the dashed line indicates the interface between the β-Ga_2O_3 (010) substrate and the grown β-Ga_2O_3 film.

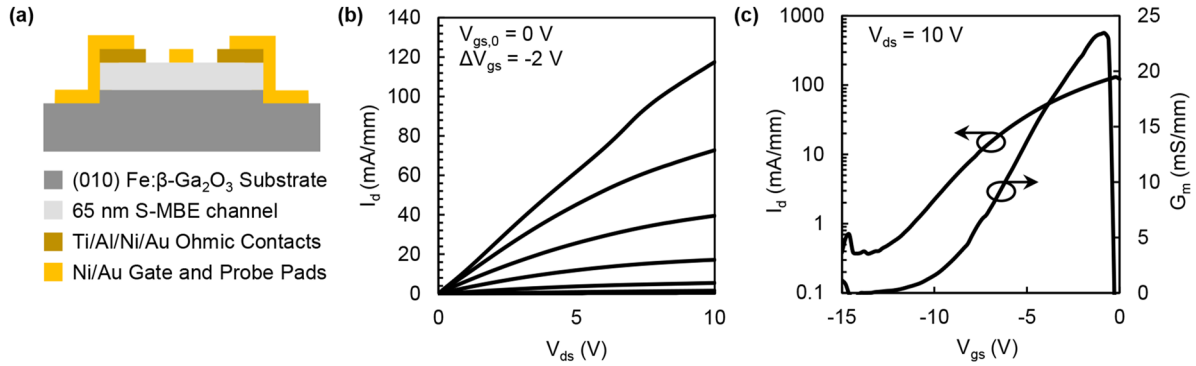

FIG. 7. (a) Schematic of the annealed-ohmic MESFET fabricated using a silicon-doped β-Ga_2O_3 film grown at ~1 μm/h by *S*-MBE with $N_d = 10^{18}$ cm^{-3}. (b) Output curves at V_{gs} = 0, −2, −4, −6, −8, and −10 V and (c) transfer curve and transconductance of the MESFET.

channel material grown by *S*-MBE is, indeed, suitable for device fabrication.

CONCLUSIONS

We have overcome the kinetic limitation to the slow growth rate of β-Ga_2O_3 by conventional MBE and demonstrate a growth rate of epitaxial β-Ga_2O_3 as high as 2.5 μm/h on (0001) Al_2O_3 substrates by *S*-MBE. By using a doping source in which silicon is in its most oxidized state, SiO_2, we avoid the oxidation issues of previously used silicon[4,5,29] and SiO dopant sources[37] when used at high oxidant pressures. This enables controllable and reproducible silicon-doping of β-Ga_2O_3 in the 5×10^{16} cm^{-3}–10^{19} cm^{-3} range for the high growth rates used. The doped films grown at ~1 μm/h exhibit mobilities at room temperature rivaling leading techniques and mobilities, at low temperatures, that are the highest achieved to date by MBE, 627 cm^2 V^{-1} s^{-1} at 76 K. While these characteristics are still inferior to the electrical properties of β-Ga_2O_3 grown by MOCVD,[2–4,23–25] *S*-MBE is emerging as a viable technique for the growth of electronic-grade β-Ga_2O_3 at rates enabling the intensive investigation of thick vertical heterostructures.

SUPPLEMENTARY MATERIAL

See the supplementary material for calculated partial pressures and additional sample data.

ACKNOWLEDGMENTS

K.A., C.A.G., N.A.P., J.S., J.P.M., D.J., H.G.X., D.A.M., M.O.T., H.P.N., and D.G.S. acknowledge the support from the AFOSR/AFRL ACCESS Center of Excellence under Award No. FA9550-18-1-0529. J.P.M. also acknowledges the support from the National Science Foundation within a Graduate Research Fellowship under Grant No. DGE-1650441. P.V. and Y.A.B. acknowledge the support from ASCENT, one of six centers in JUMP, a Semiconductor Research Corporation (SRC) program sponsored by DARPA. F.V.E.H. acknowledges the support from the Alexander von Humboldt Foundation in the form of a Feodor Lynen fellowship. F.V.E.H. also acknowledges the support from the National Science Foundation (NSF) [Platform for the Accelerated Realization, Analysis and Discovery of Interface Materials (PARADIM)] under Cooperative Agreement No. DMR-1539918. M.D.W., D.A.M., and D.G.S. acknowledge the support from the NSF under DMR-2122147. M.D.W. also acknowledges NSF Grant No. HRD-1924204 and ONR Award No. N00014-21-1-2823. This work made use of the Cornell Center for Materials Research (CCMR) Shared Facilities, which are supported through the NSF MRSEC Program (Grant No. DMR-1719875). The substrate preparation was performed, in part, at the Cornell NanoScale Facility, a member of the National Nanotechnology Coordinated Infrastructure (NNCI), which is supported by the NSF (Grant No. NNCI-2025233). This work also made use of the Cornell Energy Systems Institute Shared Facilities partly sponsored by the NSF (Grant No. MRI DMR-1338010).

AUTHOR DECLARATIONS

Conflict of Interest

The authors K.A., F.V.E.H., S.-L.S., P.V., Z.-K.L., and D.G.S. have been granted U.S. Patent No. 11,462,402 (4 October 2022) with the title "Suboxide Molecular-Beam Epitaxy and Related Structures."

Author Contributions

Kathy Azizie: Conceptualization (equal); Data curation (lead); Formal analysis (lead); Investigation (lead); Methodology (equal); Validation (lead); Visualization (lead); Writing – original draft (equal); Writing – review & editing (equal). **Felix V. E. Hensling**: Conceptualization (equal); Data curation (equal); Formal analysis (equal); Investigation (equal); Supervision (supporting); Validation (supporting); Visualization (equal); Writing – review & editing (equal). **Cameron A. Gorsak**: Data curation (equal); Formal analysis (supporting); Investigation (supporting); Methodology (supporting); Writing – review & editing (supporting). **Yunjo Kim**: Formal analysis (supporting); Investigation (supporting); Visualization (supporting). **Naomi A. Pieczulewski**: Data curation (equal); Formal analysis (supporting); Investigation (equal); Visualization (equal); Writing – original draft (supporting); Writing – review & editing (supporting). **Daniel M. Dryden**: Formal analysis (supporting);

Investigation (supporting); Visualization (equal). **M. K. Indika Senevirathna**: Formal analysis (supporting); Investigation (supporting); Visualization (equal). **Selena Coye**: Data curation (supporting); Formal analysis (supporting); Investigation (supporting); Visualization (equal). **Shun-Li Shang**: Data curation (supporting); Formal analysis (supporting); Investigation (supporting); Visualization (equal). **Jacob Steele**: Formal analysis (equal); Investigation (supporting); Methodology (equal); Visualization (equal). **Patrick Vogt**: Formal analysis (equal); Investigation (supporting); Methodology (equal); Visualization (supporting). **Nicholas A. Parker**: Formal analysis (supporting); Investigation (supporting); Visualization (supporting); Writing – original draft (supporting); Writing – review & editing (supporting). **Yorick A. Birkhölzer**: Investigation (supporting); Writing – original draft (supporting); Writing – review & editing (supporting). **Jonathan P. McCandless**: Funding acquisition (equal); Investigation (supporting); Supervision (supporting); Writing – original draft (supporting); Writing – review & editing (supporting). **Debdeep Jena**: Funding acquisition (equal); Investigation (supporting); Supervision (supporting); Writing – review & editing (supporting). **Huili G. Xing**: Data curation (supporting); Funding acquisition (equal); Supervision (supporting); Writing – review & editing (supporting). **Zi-Kui Liu**: Data curation (supporting); Investigation (supporting); Supervision (supporting). **Michael D. Williams**: Investigation (supporting); Supervision (supporting). **Andrew J. Green**: Funding acquisition (equal); Investigation (supporting); Supervision (supporting). **Kelson Chabak**: Data curation (equal); Funding acquisition (equal); Investigation (supporting); Supervision (supporting); Visualization (equal); Writing – review & editing (equal). **David A. Muller**: Funding acquisition (equal); Resources (supporting); Supervision (supporting); Visualization (supporting); Writing – review & editing (supporting). **Adam T. Neal**: Data curation (equal); Funding acquisition (equal); Investigation (supporting); Supervision (supporting); Visualization (equal); Writing – review & editing (equal). **Shin Mou**: Funding acquisition (equal); Supervision (supporting); Writing – review & editing (equal). **Michael O. Thompson**: Conceptualization (lead); Funding acquisition (equal); Investigation (equal); Project administration (lead); Resources (lead); Supervision (supporting); Validation (equal); Writing – original draft (equal); Writing – review & editing (equal). **Hari P. Nair**: Data curation (equal); Funding acquisition (equal); Investigation (equal); Supervision (supporting); Visualization (equal); Writing – original draft (supporting); Writing – review & editing (equal). **Darrell G. Schlom**: Conceptualization (lead); Funding acquisition (lead); Investigation (equal); Project administration (lead); Resources (lead); Supervision (lead); Validation (equal); Visualization (supporting); Writing – original draft (equal); Writing – review & editing (lead).

DATA AVAILABILITY

The data that support the findings of this study are available within the article and are openly available at https://doi.org/10.34863/zsda-pa72.

REFERENCES

[1] M. Higashiwaki and G. H. Jessen, "Guest Editorial: The dawn of gallium oxide microelectronics," Appl. Phys. Lett. **112**, 060401 (2018).

[2] A. J. Green, J. Speck, G. Xing, P. Moens, F. Allerstam, K. Gumaelius, T. Neyer, A. Arias-Purdue, V. Mehrotra, A. Kuramata, K. Sasaki, S. Watanabe, K. Koshi, J. Blevins, O. Bierwagen, S. Krishnamoorthy, K. Leedy, A. R. Arehart, A. T. Neal, S. Mou, S. A. Ringel, A. Kumar, A. Sharma, K. Ghosh, U. Singisetti, W. Li, K. Chabak, K. Liddy, A. Islam, S. Rajan, S. Graham, S. Choi, Z. Cheng, and M. Higashiwaki, "β-gallium oxide power electronics," APL Mater. **10**, 029201 (2022).

[3] L. Meng, Z. Feng, A. F. M. A. U. Bhuiyan, and H. Zhao, "High-mobility MOCVD β-Ga_2O_3 epitaxy with fast growth rate using trimethylgallium," Cryst. Growth Des. **22**, 3896–3904 (2022).

[4] A. Waseem, Z. Ren, H.-C. Huang, K. Nguyen, X. Wu, and X. Li, "A review of recent progress in β-Ga_2O_3 epitaxial growth: Effect of substrate orientation and precursors in metal–organic chemical vapor deposition," Phys. Status Solidi A **219**, 2200616 (2022).

[5] J. P. McCandless, V. Protasenko, B. W. Morell, E. Steinbrunner, A. T. Neal, N. Tanen, Y. Cho, T. J. Asel, S. Mou, P. Vogt, H. G. Xing, and D. Jena, "Controlled Si doping of β-Ga_2O_3 by molecular beam epitaxy," Appl. Phys. Lett. **121**, 072108 (2022).

[6] A. Mauze, Y. Zhang, T. Itoh, E. Ahmadi, and J. S. Speck, "Sn doping of (010) β-Ga_2O_3 films grown by plasma-assisted molecular beam epitaxy," Appl. Phys. Lett. **117**, 222102 (2020).

[7] P. Vogt and O. Bierwagen, "The competing oxide and sub-oxide formation in metal-oxide molecular beam epitaxy," Appl. Phys. Lett. **106**, 081910 (2015).

[8] P. Vogt and O. Bierwagen, "Reaction kinetics and growth window for plasma-assisted molecular beam epitaxy of Ga_2O_3: Incorporation of Ga vs. Ga_2O desorption," Appl. Phys. Lett. **108**, 072101 (2016).

[9] P. Vogt and O. Bierwagen, "Quantitative subcompound-mediated reaction model for the molecular beam epitaxy of III-VI and IV-VI thin films: Applied to Ga_2O_3, In_2O_3, and SnO_2," Phys. Rev. Mater. **2**, 120401 (2018).

[10] P. Vogt, O. Brandt, H. Riechert, J. Lähnemann, and O. Bierwagen, "Metal-exchange catalysis in the growth of sesquioxides: Towards heterostructures of transparent oxide semiconductors," Phys. Rev. Lett. **119**, 196001 (2017).

[11] P. Vogt, A. Mauze, F. Wu, B. Bonef, and J. S. Speck, "Metal-oxide catalyzed epitaxy (MOCATAXY): The example of the O plasma-assisted molecular beam epitaxy of β-$(Al_xGa_{1-x})_2O_3$/β-Ga_2O_3 heterostructures," Appl. Phys. Express **11**, 115503 (2018).

[12] P. Mazzolini, A. Falkenstein, C. Wouters, R. Schewski, T. Markurt, Z. Galazka, M. Martin, M. Albrecht, and O. Bierwagen, "Substrate-orientation dependence of β-Ga_2O_3 (100), (010), (001), and $(\bar{2}01)$omoepitaxy by indium-mediated metal-exchange catalyzed molecular beam epitaxy (MEXCAT-MBE)," APL Mater. **8**, 011107 (2020).

[13] M. Kracht, A. Karg, J. Schörmann, M. Weinhold, D. Zink, F. Michel, M. Rohnke, M. Schowalter, B. Gerken, A. Rosenauer, P. J. Klar, J. Janek, and M. Eickhoff, "Tin-assisted synthesis of ε-Ga_2O_3 by molecular beam epitaxy," Phys. Rev. Appl. **8**, 054002 (2017).

[14] P. Vogt, F. V. E. Hensling, K. Azizie, C. S. Chang, D. Turner, J. Park, J. P. McCandless, H. Paik, B. J. Bocklund, G. Hoffman, O. Bierwagen, D. Jena, H. G. Xing, S. Mou, D. A. Muller, S.-L. Shang, Z.-K. Liu, and D. G. Schlom, "Adsorption-controlled growth of Ga_2O_3 by suboxide molecular-beam epitaxy," APL Mater. **9**, 031101 (2021).

[15] S. Ghose, M. S. Rahman, J. S. Rojas-Ramirez, M. Caro, R. Droopad, A. Arias, and N. Nedev, "Structural and optical properties of β-Ga_2O_3 thin films grown by plasma-assisted molecular beam epitaxy," J. Vac. Sci. Technol. B **34**, 02L109 (2016).

[16] S. Ghose, S. Rahman, L. Hong, J. S. Rojas-Ramirez, H. Jin, K. Park, R. Klie, and R. Droopad, "Growth and characterization of β-Ga_2O_3 thin films by molecular beam epitaxy for deep-UV photodetectors," J. Appl. Phys. **122**, 095302 (2017).

[17] C. J. Frosch and C. D. Thurmond, "The pressure of Ga_2O over gallium-Ga_2O_3 mixtures," J. Phys. Chem. **66**, 877–878 (1962).

[18] G. Hoffmann, M. Budde, P. Mazzolini, and O. Bierwagen, "Efficient suboxide sources in oxide molecular beam epitaxy using mixed metal + oxide charges: The examples of SnO and Ga_2O," APL Mater. **8**, 031110 (2020).

[19] K. M. Adkison, S.-L. Shang, B. J. Bocklund, D. Klimm, D. G. Schlom, and Z.-K. Liu, "Suitability of binary oxides for molecular-beam epitaxy source materials: A comprehensive thermodynamic analysis," APL Mater. **8**, 081110 (2020).

[20]M. Passlack, J. K. Abrokwah, R. Droopad, and C. D. Overgaard, "III-V epitaxial wafer production," U.S. patent 6,030,453 (February 29, 2000).
[21]M. Passlack, J. K. Abrokwah, and Z. J. Yu, "Ultraviolet transmitting oxide with metallic oxide phase and method of fabrication," U.S. patent 6,094,295 (July 25, 2000).
[22]M. Passlack, Z. Yu, R. Droopad, J. K. Abrokwah, D. Braddock, S.-I. Yi, M. Hale, J. Sexton, and A. C. Kummel, "Gallium oxide on gallium arsenide: Atomic structure, materials, and devices," in *III-V Semiconductor Heterostructures: Physics and Devices*, edited by W. Z. Cai (Research Signpost, Kerala, India, 2003), pp. 1–29.
[23]F. Alema, Y. Zhang, A. Osinsky, N. Valente, A. Mauze, T. Itoh, and J. S. Speck, "Low temperature electron mobility exceeding 10^4 cm^2/V s in MOCVD grown β-Ga_2O_3," APL Mater. **7**, 121110 (2019).
[24]Z. Feng, A. F. M. A. U. Bhuiyan, Z. Xia, W. Moore, Z. Chen, J. F. McGlone, D. R. Daughton, A. R. Arehart, S. A. Ringel, S. Rajan, and H. Zhao, "Probing charge transport and background doping in metal-organic chemical vapor deposition-grown (010) β-Ga_2O_3," Phys. Status Solidi RRL **14**, 2000145 (2020).
[25]A. Bhattacharyya, C. Peterson, T. Itoh, S. Roy, J. Cooke, S. Rebollo, P. Ranga, B. Sensale-Rodriguez, and S. Krishnamoorthy, "Superior electron mobility in Si-doped (010) β-Ga_2O_3 films with low-temperature buffer layers," APL Mater. **11**, 021110 (2023)
[26]M. Baldini, Z. Galazka, and G. Wagner, "Recent progress in the growth of β-Ga_2O_3 for power electronics applications," Mater. Sci. Semicond. Process. **78**, 132–146 (2018).
[27]Z. Feng, A. F. M. A. U. Bhuiyan, M. R. Karim, and H. Zhao, "MOCVD homoepitaxy of Si-doped (010) β-Ga_2O_3 thin films with superior transport properties," Appl. Phys. Lett. **114**, 250601 (2019).
[28]R. Sharma, M. E. Law, F. Ren, A. Y. Polyakov, and S. J. Pearton, "Diffusion of dopants and impurities in β-Ga_2O_3," J. Vac. Sci. Technol. A **39**, 060801 (2021).
[29]N. K. Kalarickal, Z. Xia, J. McGlone, S. Krishnamoorthy, W. Moore, M. Brenner, A. R. Arehart, S. A. Ringel, and S. Rajan, "Mechanism of Si doping in plasma assisted MBE growth of β-Ga_2O_3," Appl. Phys. Lett. **115**, 152106 (2019).
[30]J. J. Lander and J. Morrison, "Low voltage electron diffraction study of the oxidation and reduction of silicon," J. Appl. Phys. **33**, 2089–2092 (1962).
[31]F. W. Smith and G. Ghidini, "Reaction of oxygen with Si(111) and (100): Critical conditions for the growth of SiO_2," J. Electrochem. Soc. **129**, 1300–1306 (1982).
[32]D. Starodub, E. P. Gusev, E. Garfunkel, and T. Gustafsson, "Silicon oxide decomposition and desorption during the thermal oxidation of silicon," Surf. Rev. Lett. **06**, 45–52 (1999).
[33]P. Vogt, F. V. E. Hensling, K. Azizie, J. P. McCandless, J. Park, K. DeLello, D. A. Muller, H. G. Xing, D. Jena, and D. G. Schlom, "Extending the kinetic and thermodynamic limits of molecular-beam epitaxy utilizing suboxide sources or metal-oxide-catalyzed epitaxy," Phys. Rev. Appl. **17**, 034021 (2022).
[34]Scientific Group Thermodata Europe (SGTE), in *Landolt-Börnstein: Numerical Data and Functional Relationships in Science and Technology, New Series, Group IV*, edited by Lehrstuhl für Theoretische Hüttenkunde (Springer-Verlag, Berlin, Heidelberg, 1999), Vol. 19a.
[35]J.-O. Andersson, T. Helander, L. Höglund, P. Shi, and B. Sundman, "Thermo-Calc & DICTRA, computational tools for materials science," Calphad **26**, 273–312 (2002).
[36]P. Vogt, D. G. Schlom, F. V. E. Hensling, K. Azizie, Z.-K. Liu, B. J. Bocklund, and S.-L. Shang, "Suboxide molecular-beam epitaxy and related structures," U.S. patent 11,462,402 (October 4, 2022).
[37]A. Ardenghi, O. Bierwagen, A. Falkenstein, G. Hoffmann, J. Lähnemann, M. Martin, and P. Mazzolini, "Toward controllable Si-doping in oxide molecular beam epitaxy using a solid SiO source: Application to β-Ga_2O_3," Appl. Phys. Lett. **121**, 042109 (2022).
[38]H. Okumura, "Sn and Si doping of α-Al_2O_3 (10-10) layers grown by plasma-assisted molecular beam epitaxy," Jpn. J. Appl. Phys. **61**, 125505 (2022).
[39]L. J. van der Pauw, "A method of measuring specific resistivity and Hall effect of discs of arbitrary shape," Philips Res. Rep. **20**, 220–224 (1958).
[40]A. J. Green, K. D. Chabak, E. R. Heller, R. C. Fitch, M. Baldini, A. Fiedler, K. Irmscher, G. Wagner, Z. Galazka, S. E. Tetlak, A. Crespo, K. Leedy, and G. H. Jessen, "3.8-MV/cm breakdown strength of MOVPE-grown Sn-doped β-Ga_2O_3 MOSFETs," IEEE Electron Device Lett. **37**, 902–905 (2016).
[41]M. Orita, H. Hiramatsu, H. Ohta, M. Hirano, and H. Hosono, "Preparation of highly conductive, deep ultraviolet transparent β-Ga_2O_3 thin film at low deposition temperatures," Thin Solid Films **411**, 134–139 (2002).
[42]V. Gottschalch, K. Mergenthaler, G. Wagner, J. Bauer, H. Paetzelt, C. Sturm, and U. Teschner, "Growth of β-Ga_2O_3 on Al_2O_3 and GaAs using metal-organic vapor-phase epitaxy," Phys. Status Solidi A **206**, 243–249 (2009).
[43]E. G. Víllora, K. Shimamura, K. Kitamura, and K. Aoki, "Rf-plasma-assisted molecular-beam epitaxy of β-Ga_2O_3," Appl. Phys. Lett. **88**, 031105 (2006).
[44]T. Oshima, T. Okuno, and S. Fujita, "Ga_2O_3 thin film growth on *c*-plane sapphire substrates by molecular beam epitaxy for deep-ultraviolet photodetectors," Jpn. J. Appl. Phys. **46**, 7217–7220 (2007).
[45]M. Yasaka, "X-ray thin-film measurement techniques V. X-ray reflectivity measurement," Rigaku J. **26**, 1–9 (2010).
[46]G. Hass, "Preparation, structure, and applications of thin films of silicon monoxide and titanium dioxide," J. Am. Ceram. Soc. **33**, 353–360 (1950).
[47]E. Ahmadi, O. S. Koksaldi, X. Zheng, T. Mates, Y. Oshima, U. K. Mishra, and J. S. Speck, "Demonstration of β-$(Al_xGa_{1-x})_2O_3$/β-Ga_2O_3 modulation doped field-effect transistors with Ge as dopant grown via plasma-assisted molecular beam epitaxy," Appl. Phys. Express **10**, 071101 (2017).
[48]T. Kamimura, Y. Nakata, M. H. Wong, and M. Higashiwaki, "Normally-off Ga_2O_3 MOSFETs with unintentionally nitrogen-doped channel layer grown by plasma-assisted molecular beam epitaxy," IEEE Electron Device Lett. **40**, 1064–1067 (2019).
[49]T. J. Asel, E. Steinbrunner, J. Hendricks, A. T. Neal, and S. Mou, "Reduction of unintentional Si doping in β-Ga_2O_3 grown via plasma-assisted molecular beam epitaxy," J. Vac. Sci. Technol. A **38**, 043403 (2020).
[50]A. Mauze, Y. Zhang, T. Mates, F. Wu, and J. S. Speck, "Investigation of unintentional Fe incorporation in (010) β-Ga_2O_3 films grown by plasma-assisted molecular beam epitaxy," Appl. Phys. Lett. **115**, 052102 (2019).
[51]L. P. Firsova and A. N. Nesmeyanov, "Determination of the coefficients of condensation of lithium, beryllium, boron, silicon and lead oxides," Zh. Fiz. Khim. **34**, 2719–2722 (1960).
[52]S.-I. Nagai, K. Niwa, M. Shinmei, and T. Yokokawa, "Knudsen effusion study of silica," J. Chem. Soc., Faraday Trans. 1 **69**, 1628–1634 (1973).
[53]S. I. Shornikov, I. Y. Archakov, and M. M. Shul'tz, "Mass spectrometric study of vaporization and thermodynamic properties of silicon dioxide: II. Determination of partial vaporization coefficients of silicon dioxide," Russ. J. Gen. Chem. **69**, 187–196 (1999).
[54]Y. Zhang, Z. Feng, M. R. Karim, and H. Zhao, "High-temperature low-pressure chemical vapor deposition of β-Ga_2O_3," J. Vac. Sci. Technol. A **38**, 050806 (2020).
[55]K. Goto, K. Konishi, H. Murakami, Y. Kumagai, B. Monemar, M. Higashiwaki, A. Kuramata, and S. Yamakoshi, "Halide vapor phase epitaxy of Si doped β-Ga_2O_3 and its electrical properties," Thin Solid Films **666**, 182–184 (2018).
[56]A. T. Neal, S. Mou, R. Lopez, J. V. Li, D. B. Thomson, K. D. Chabak, and G. H. Jessen, "Incomplete ionization of a 110 meV unintentional donor in β-Ga_2O_3 and its effect on power devices," Sci. Rep. **7**, 13218 (2017).
[57]A. T. Neal, S. Mou, S. Rafique, H. Zhao, E. Ahmadi, J. S. Speck, K. T. Stevens, J. D. Blevins, D. B. Thomson, N. Moser, K. D. Chabak, and G. H. Jessen, "Donors and deep acceptors in β-Ga_2O_3," Appl. Phys. Lett. **113**, 062101 (2018).
[58]H. M. Jeon, K. D. Leedy, D. C. Look, C. S. Chang, D. A. Muller, S. C. Badescu, V. Vasilyev, J. L. Brown, A. J. Green, and K. D. Chabak, "Homoepitaxial β-Ga_2O_3 transparent conducting oxide with conductivity σ = 2323 S cm^{-1}," APL Mater. **9**, 101105 (2021).
[59]M. Higashiwaki, K. Sasaki, A. Kuramata, T. Masui, and S. Yamakoshi, "Gallium oxide (Ga_2O_3) metal-semiconductor field-effect transistors on single-crystal β-Ga_2O_3 (010) substrates," Appl. Phys. Lett. **100**, 013504 (2012).